Effects of Breathing and Cardiac Motion on Spatial Resolution in the Microscopic Imaging of Rodents

Wilfried Maï, Cristian T. Badea, Charles T. Wheeler, Laurence W. Hedlund, and G. Allan Johnson*

One can acquire high-resolution pulmonary and cardiac images in live rodents with MR microscopy by synchronizing the image acquisition to the breathing cycle across multiple breaths, and gating to the cardiac cycle. The precision with which one can synchronize image acquisition to the motion defines the ultimate resolution limit that can be attained in such studies. The present work was performed to evaluate how reliably the pulmonary and cardiac structures return to the same position from breath to breath and beat to beat across the prolonged period required for MR microscopy. Radiopaque beads were surgically glued to the abdominal surface of the diaphragm and on the cardiac ventricles of anesthetized, mechanically ventilated rats. We evaluated the range of motion for the beads (relative to a reference vertebral bead) using digital microradiography with two specific biological gating methods: 1) ventilation synchronous acquisition, and 2) both ventilation synchronous *and* cardiac-gated acquisitions. The standard deviation (SD) of the displacement was ≤100 μm, which is comparable to the resolution limit for in vivo MRI imposed by signal-to-noise ratio (SNR) constraints. With careful control of motion, its impact on resolution can be limited. This work provides the first quantitative measure of the motion-imposed resolution limits for in vivo imaging. Magn Reson Med 53:858–865, 2005. © 2005 Wiley-Liss, Inc.

Key words: resolution; motion; rodent; magnetic resonance imaging; digital microradiography

Numerous authors have discussed potential resolution barriers for magnetic resonance imaging (MRI). At the most fundamental level, resolution is limited by the physics of diffusion and susceptibility (1,2). At a more practical level, the spatial resolution is limited by the available signal (3). We believe that in in vivo studies, particularly in the thoracic cavity, the fundamental resolution limit is imposed by motion. A number of gating strategies are used to limit the impact of motion, including ventilatory synchronization (4,5), cardiac gating (6), and radial encoding (7). However, the fundamental resolution limit on any study employing synchronous and/or gated acquisition is determined by the reliability of the gating in capturing the moving anatomy at the same point in the physiologic cycle.

Center for In Vivo Microscopy, Duke University Medical Center, Durham, North Carolina.

Grant sponsor: NCRR; Grant number: P41 RR05959; Grant sponsor: NCI; Grant number: R24 CA-92656; Grant sponsor: Department of Defense; Grant number: DoD-556450; Grant sponsor: French Ministry of Foreign Affairs.

*Correspondence to: G. Allan Johnson, Center for In Vivo Microscopy, Box 3302, Duke University Medical Center, Durham, NC 27710.
E-mail: gaj@orion.duhs.duke.edu

Received 27 August 2004; revised 20 October 2004; accepted 22 October 2004.

DOI 10.1002/mrm.20400
Published online in Wiley InterScience (www.interscience.wiley.com).

The lung is one of the most challenging organs to image, in part because of magnetic susceptibility, low proton density, and motion (8). In particular, constant motion from breathing and cardiac activity produces blurring and ghosting artifacts, which can seriously degrade image quality (4,9,10). New strategies have been developed to overcome these issues, and in vivo MR images of the lung in rodents have been acquired with a Nyquist limited resolution of <100 μm (11).

MRI has also proven to be a highly accurate and reproducible method for assessing cardiac morphology and function in rodents (12–14). Studies have been performed by optimizing pulse sequences and developing specific monitoring and gating systems adapted to the requirements of small, rapidly beating mouse and rat hearts (12,13,15).

With the increased interest in imaging the hearts and lungs of small animals, a persistent question that arises is, what are the motion-imposed resolution limits? To address this question, we evaluated the reliability of repositioning the diaphragm and heart over a number of breathing and cardiac cycles in mechanically ventilated rats using a high-resolution digital X-ray system with various combinations of cardiac gating and breathing synchronization. Finally, we tested the best combinations with MRI to demonstrate how these combinations would improve MR spatial resolution for small-animal imaging.

MATERIALS AND METHODS

Surgical Preparation of Animals

For these studies we used male Fisher 344 rats (150–200 g), following procedures approved by the Duke Institutional Animal Care and Use Committee. For the diaphragm motion studies ($N = 10$), tungsten beads were glued to the abdominal surface of the diaphragm. The animals were first anesthetized with methohexital (40 mg/kg, IP), perorally intubated, and mechanically ventilated. Anesthesia was maintained with isoflurane (2–3%; Halocarbon Laboratories, River Edge, NJ) and body temperature was maintained with a heating pad. Through a midline incision, three tungsten beads (0.28 mm in diameter; New England Miniature Ball LLC, Norfolk, CT) were glued (cyanoacrylate) to the abdominal surface of the diaphragm. Each bead was first glued to a small teardrop-shaped piece of filter paper to ease handling with forceps. One bead was placed on the dome of the diaphragm in the region of closest contact with the cardiac apex, and the two other beads were placed laterally on the left and right sides of the dome. The muscle and skin layers were then closed with silk sutures. A reference bead was also glued to a thoracic vertebrae through a dorsal midline incision. Fol-

lowing a ventral incision in the neck, a ligature was tied around the trachea to prevent air leakage during brief breath-holds. Once prepared, these animals were used immediately for the X-ray imaging experiment.

In preparation for cardiac motion studies ($N = 3$), three or four tungsten beads (see above) were glued to the right and left ventricular surfaces. For this aseptic surgery, the rats were anesthetized, intubated, and ventilated as described above. Through a left intercostal incision, beads were glued (see above) to the surface of the right and left ventricles at the maximum lateral width of the heart, as well as one at the midline position and one at the apex. After residual pleural air was aspirated, the chest wall was closed with monofilament suture and the skin was closed with wound clips. A reference bead was also glued to a thoracic vertebrae as described above. The animals were then given a subcutaneous injection of 0.3 mg/kg buprenorphine (Buprenex; Reckitt Benckiser Pharmaceuticals Inc., Richmond, VA) before recovery, and then every 12 hr for 3 days after surgery. X-ray studies were performed 10–15 days after surgery to allow the animals to recover fully.

Preparation of Animals for Imaging

All of the animals were prepared similarly for both the X-ray and MRI studies. First, the animals were anesthetized with methohexital (40 mg/kg, IP, Brevital; Eli Lilly, Indianapolis, IN), perorally intubated, and mechanically ventilated with an MR-compatible ventilator (16) at 60 breaths per minute with a tidal volume of 1.8–3.0 ml. Anesthesia was maintained with isoflurane (2–3%), and body temperature was maintained at normal levels with a feedback-controlled heat lamp and a heated-air feedback system for X-ray and MRI, respectively (17). A solid-state pressure transducer on the breathing valve measured airway pressure. Pediatric electrodes were taped on the footpads for ECG. Body temperature was recorded with a rectal thermistor. All physiologic signals were processed (Coulbourn Instruments, Allentown, PA) and displayed on a computer using LabVIEW software (National Instruments, Austin, TX) for continuous monitoring during the experiment. These signals were also used to control the gating described below. At the conclusion of the studies for diaphragm motion, the animals were euthanized with an overdose of anesthesia. However, the rats prepared with cardiac beads were allowed to recover and were then reimaged two or three more times before they were sacrificed. These additional imaging sessions were always separated by at least 1 week. The animals were prepared as described above for these additional imaging sessions, and after the final session the animals were sacrificed by anesthesia overdose. At the completion of MRI, the animals were euthanized by tail vein injection of KCl.

Digital X-Ray Acquisition

Radiographic images were acquired with a digital X-ray system developed for microradiography of rats and mice. The system includes a high-capacity (9/50 kW) angiography tube with 0.3/1.0 mm focal spots powered by a Phillips CXP 80 generator. The tube, detector, and support are mounted on an extruded aluminum gantry that allows flexible placement of the tube, detector, and animal to limit penumbral blur to less than the Nyquist sample of the detector. The animals were positioned supine on a custom-designed table that allows the three major axes to be changed without disturbing the animal. Ventrodorsal (vertical X-ray beam) and lateral (horizontal X-ray beam) projections were acquired. The X-ray settings were as follows: 85 kV, 80 mA, 15 ms for the diaphragm motion study; and 80 kV, 100 mA, 5.5 ms for the cardiac motion study. The digital camera (Microphotonics XQUIS; Photonics Science, East Sussex, UK) had an in-plane resolution of 50 μm, image matrix size of 1024×1024, and a field of view (FOV) of 51.2×51.2 mm. In one diaphragm-motion experiment we used a different camera, but of the same type, with an in-plane resolution of 20 μm and image matrix of 1024×1024 (FOV = 20.48×20.48 mm).

Gating Methods

LabVIEW applications, written in-house, were used to monitor the physiologic parameters, and control ventilation and image acquisition. For the X-ray studies, the LabVIEW application controlled exposure, camera readout, and image storage. This imaging sequence consisted of a series of events, including X-ray generation, image acquisition, and storage, which were initiated by specific triggers from biological signals, such as the QRS of the ECG and/or phase of the ventilation cycle in a fashion similar to the series of events associated with an MR image acquisition sequence. For each X-ray sequence, a series of 150–200 images were acquired with each exposure initiated by either the ventilation or the cardiac triggers. However, instead of acquiring a single line of Fourier space on each acquisition (as performed in MRI), we acquired 2D radiographic projections. Two different gating methods were used: ventilation synchronous exposures without cardiac gating, and ventilation synchronous exposures with cardiac gating (7,18).

To study the impact of breathing motion, we obtained a series of images at two points of the breathing cycle (Fig. 1). A delay was inserted between the initial ventilation trigger, which started inspiration, and the radiographic exposure and camera readout. Depending on the duration of this delay, an X-ray pulse and camera read/store were generated either during the brief breath-hold at full inspiration or during end-expiration. The 15-ms radiographic exposure was comparable to an MR image acquired at 34 kHz.

To study the impact of cardiac motion on the diaphragm, we defined an image acquisition window of 110-ms duration during the two phases of the breathing cycle as described above (brief breath-hold at full inspiration and at end-expiration) (Fig. 2). The first QRS spike that occurred within this window triggered a 5.5-ms X-ray exposure. Thus, the images were always acquired at the same phase of the cardiac cycle and during the same phase of ventilation. For breath-hold images, the window started 250 ms after the beginning of inspiration. For end-expiration images, the acquisition window started 750 ms (early end-expiration) or 850 ms (late end-expiration) after the beginning of the inspiration.

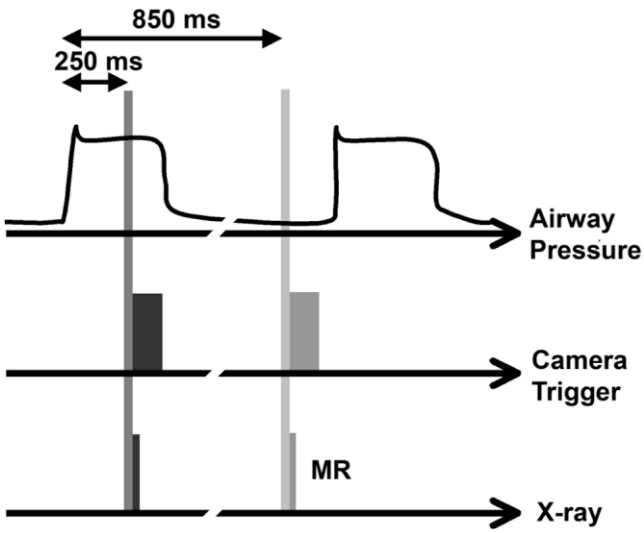

FIG. 1. The schematic for ventilation-synchronous acquisition is shown. For imaging during breath-hold, the X-ray exposure occurs 150 ms (early breath-hold) to 250 ms (late breath-hold) after the beginning of inspiration (dark gray elements). For end-expiratory images, the X-ray exposure occurs 850 ms after the beginning of the inspiration. The 5–15-ms X-ray exposure is followed by a 100-ms readout period for the camera.

To study the reproducibility of cardiac motion, we acquired images during end-expiration with the acquisition window starting 800 ms after the beginning of inspiration. Two types of experiments were performed: 1) images were acquired coincident with the QRS (pre-systole), and 2) images were acquired after a delay from the first QRS that occurred within the window. The delay was calculated depending on the heart rate, so that the X-ray exposure occurred about at a point two-thirds into the R-R interval (end-diastole).

MRI

MR images to compare the several methods of gating were acquired on a 2.0 T horizontal bore magnet (Oxford Instruments, Oxford, UK) with a GE 5X Signa console (Epic 5X; GE Healthcare, Milwaukee, WI) using a 60-mm birdcage coil. Projection encoding was used to limit phase ghosting, which is common in Cartesian encoding, so that we could obtain a more careful measure of the motion blur. For imaging, the rats ($N = 2$) were prepared, anesthetized, and monitored as described above, with the addition of a catheter placed in the lateral tail vein. In vivo images were obtained with four different gating schemes: 1) synchronous with ventilation at end-expiration and with cardiac gating on the QRS spike, 2) no gating, 3) synchronous with ventilation at end-expiration only, and 4) cardiac gating only. After these images were acquired, and without moving the animals, the rats were euthanized in the magnet by means of a tail vein injection of KCl to instantly stop the heart. A final ex vivo image was then obtained. Images were acquired in the mid-sagittal plane to allow clear delineation of the edges of both the diaphragm and the heart against the relatively low signal of the lung. The other imaging parameters were as follows: slice = 2 mm; FOV in x and y = 50 mm; number of radial views = 3200; number of points per view = 358, and TR = 500 ms. The spatial resolution in the reconstructed images was 200 μm. Since the radial encoding method images the free induction decay (FID), the effective TE is the first time point after the excitation (in this case at 852 μs). Each acquisition took approximately 30 min. To demonstrate relative blurring associated with each gating scheme, line profiles of signal intensity were generated from the images shown. These plots were based on single-pixel-wide lines at right angles to the cardiac ventricles into the lung, and at right angles to the diaphragm/liver into the lung.

Data Analysis

Using MATLAB (The Mathworks Inc., Natick, MA), we drew rectangular regions of interest (ROIs) around each bead and segmented the pixels corresponding to the bead by thresholding. The coordinates of the center of each bead were then calculated as the average of the coordinates of these segmented pixels on both the x- and y-axes. Based on

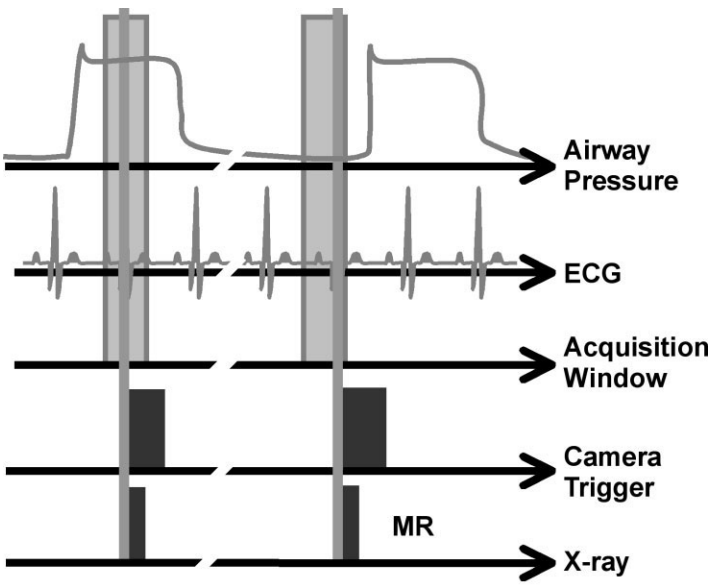

FIG. 2. The schematic for ventilation-synchronous acquisition with cardiac gating is shown. A 110-ms acquisition window is defined and any QRS that occurs within this window triggers an X-ray exposure and enables the camera to acquire the data. The window can be placed at any point in the ventilation cycle, e.g., at breath-hold (left) or at end expiration (right). An independent (additional) delay allows the exposure to be triggered at systole or diastole (such delays were used in the cardiac motion study). MR images were acquired only at end-expiration.

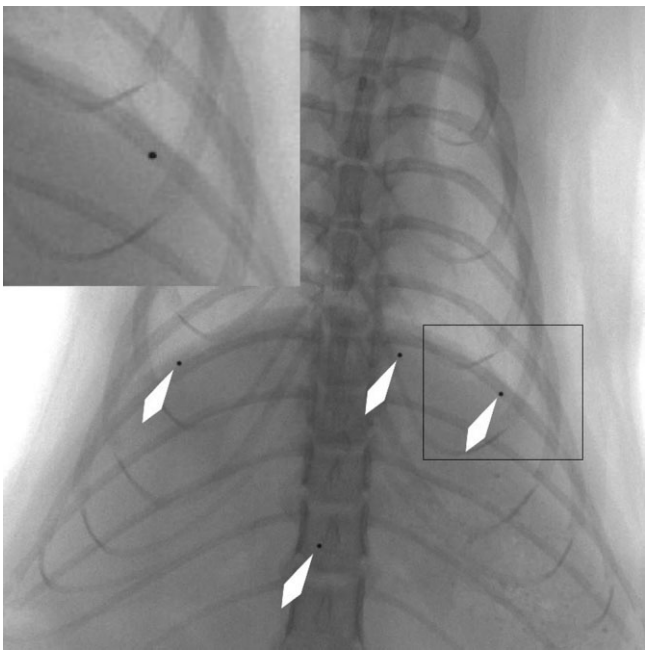

FIG. 3. Ventrodorsal projection radiograph of the thorax in a rat shows the three implanted beads on the diaphragm, as well as the reference bead on a thoracic vertebra (white arrows). A magnified view of the left bead is shown in the inset.

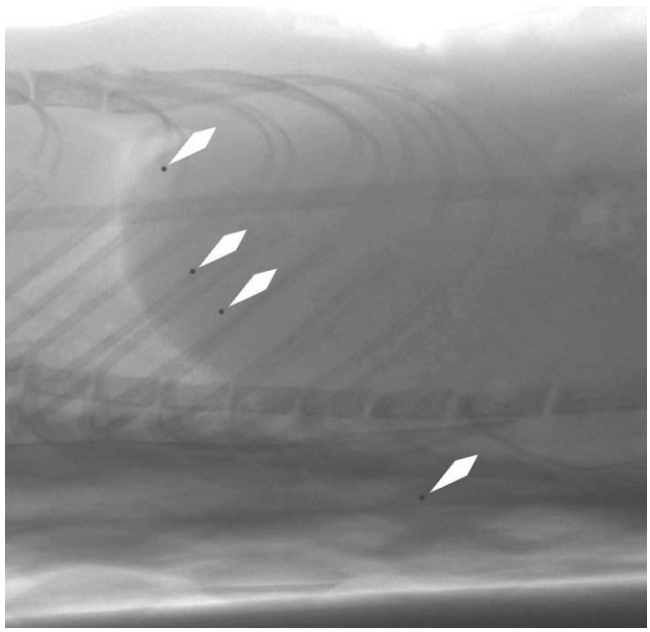

FIG. 4. Lateral (cross-table) projection radiograph of the thorax in a rat shows the three implanted beads on the diaphragm, as well as the reference bead on a thoracic vertebra (white arrows).

the coordinates of these centers, we calculated the distance in pixels between the reference vertebral bead and the diaphragmatic or cardiac beads on each image. We then calculated the standard deviation (SD) for each distance measured from 150–200 images per projection for each gating scheme.

RESULTS

Figure 3 shows a representative ventrodorsal radiograph from the study of diaphragm motion. Figure 4 shows the lateral projection. Because of the proximity to the heart, we hypothesized that the bead on the dome of the diaphragm would demonstrate a different behavior regarding its motion over time than the laterally positioned beads. The results for the dome beads are therefore shown individually in comparison with the values obtained for the beads on the lateral parts of the diaphragm. For each animal, we obtained an SD of the dome and lateral-bead motion for a sequence of 150–200 images. Figure 5 shows representative data from seven different animals to evaluate the variability (i.e., the SD) of the diaphragm motion in the ventrodorsal projection during scan synchronous ventilation at late breath-hold. Each bar represents the variability of one dome bead or two lateral beads from each animal, using 150–200 images. Since the variability in some cases (animal 1) was less than a single pixel, data were acquired (animal 2) with the higher-resolution (20-μm) camera to ensure that the algorithm locating the center of the beads was capable of subpixel accuracy. Since it was functionally much easier to locate the beads and anatomical reference points with the larger FOV in the 50-μm camera, the 20-μm camera was only used for three studies, all of which provided data consistent with the measurements from the 50-μm camera. The variability ranged from a low of <20 μm to a high of ~130 μm, which represents the degree of biologic variation.

To get some sense of the differences resulting from the four different types of gating schemes, we pooled the data for each type of scheme. Table 1 summarizes the results for multiple animals. In each case, the SD is the average across animals (ventrodorsal and lateral) for each gating scheme. As one might expect, the variability is less for the lateral beads and greater for the beads on the dome. There is little

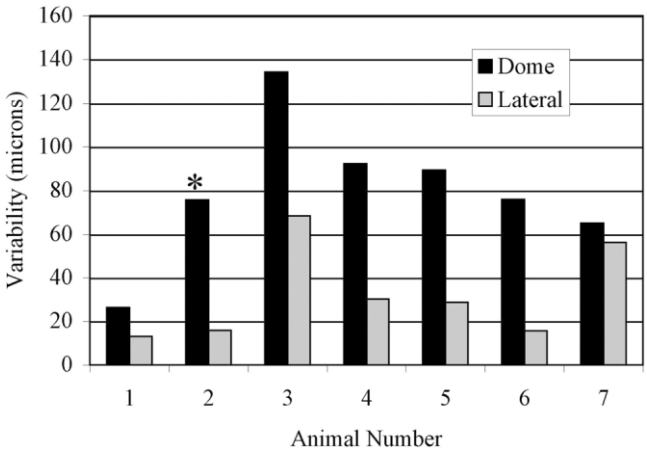

FIG. 5. Variability (i.e., SD) in displacement of the dome and lateral beads with ventilation synchronization is shown at late breath-hold. Results are presented for the ventrodorsal projection. The measurements on animal 2 were obtained with a camera with a 20-μm pitch (*). All other measurements were obtained over the entire FOV of the rat thorax using a camera with a 50-μm pitch.

Table 1
Global Results of Diaphragm Motion Study*

Gating scheme	Bead position (SD, microns)			
	Dome bead		Lateral beads	
	Ventrodorsal projection	Lateral projection	Ventrodorsal projection	Lateral projection
Ventilation synchronous/early breath-hold ($N = 4$)	69.6	71.7	37	39.4
Ventilation synchronous/late breath-hold ($N = 7$)	79.8	77.6	32.5	49.8
Ventilation synchronous/late expiration (N = 7)	99.8	40.6	25.8	25.2
Ventilation synchronous and cardiac-gated/late breath-hold ($N = 4$)	101.5	112.6	44.9	80.1
Ventilation synchronous and cardiac-gated/late expiration ($N = 4$)	90.9	43.3	34.9	46.1
Ventilation synchronous and cardiac-gated/early expiration ($N = 3$)	26.8	56.5	29.5	45.3

*For each gating scheme, the SD in microns is averaged across all animals.

dependence on the specific part of the ventilatory cycle, except in the case of cardiac-gated studies with acquisition in early expiration.

Table 2 reports the mean differences in the distances of the dome and lateral beads between the diaphragm at full-inspiration and end-expiration, as measured from both ventrodorsal and lateral projections. These data show the diaphragm excursion over the breathing cycle, providing an insight into the actual limits of spatial resolution that would be achieved without control of breathing motion. These data also allow one to put the reproducibility in Table 1 into context. For the worst case (ventilation synchronous with cardiac gating during breath-hold), the dome of the diaphragm varies in return to the equilibrium position with an SD of 101 μm or ~5% of the total motion along the longitudinal axis of the animal (2036 μm). For the best case (ventilation synchronous at expiration at the lateral portion of the diaphragm), the reproducibility of the bead positions is better than 30 μm (~3% of the excursion of the lateral beads along the *z*-axis).

For the cardiac motion studies, the number of beads glued to the heart in any of the animals ranged between three and four. Three animals were imaged with gating on the QRS at end-expiration (for a total of eight studies). Three animals were imaged with gating about two-thirds into RR interval at end-expiration (total of seven studies). Table 3 summarizes the reproducibility of the cardiac motion. For each experiment, we obtained an SD of all of the cardiac beads for a sequence of 150–200 images. The SD is roughly equivalent for both the ventrodorsal and lateral projections. There is no significant difference between the variability measured at pre-systole and diastole. The most notable feature is that the variability in the reproducibility of the heart is <50 μm, which is less than the variability of the position of the diaphragm. Since the total travel of the heart is less than the total travel of the diaphragm, this finding makes sense.

Table 2
Mean Differences (± SD), in Microns, in Distances Between Breath-Hold at Full Inspiration and End-Expiration Images

	Ventrodorsal projection	Cross-table projection
Dome	2036 (± 435)	1456 (± 221)
Lateral	859 (± 510)	689 (± 430)

Figure 6 shows a comparison of the MR images acquired in vivo with four different schemes of gating and synchronization. An image from a dead animal is also shown. Because projection encoding is relatively immune to motion artifacts, Fig. 6a, which was acquired with no gating, might be considered acceptable for imaging the spine or nonthoracic regions. On careful inspection, it is apparent that the boundary between the thorax and liver is the summation of a number of positions. The use of ventilatory synchronization without cardiac gating (Fig. 6b) improves the definition of the diaphragm edge while it leaves the cardiac boundaries poorly defined. The use of cardiac gating without ventilatory synchronization (Fig. 6c) is even less effective because of lung-related motion of the heart. In Fig. 6d, one sees the true utility of the simultaneous use of ventilatory synchronization and cardiac gating. Not only are the cardiac and diaphragm edges well defined, the pulmonary anatomy is also visible. Note that the lobar bronchus and peribronchial vessels are clearly visible here, but not in the other images.

Figure 7 summarizes quantitatively the qualitative assessments made from the MR images in Fig. 6. The line profiles crossing the edges of the diaphragm/liver to the lung, and the ventricle to the lung (Fig. 7b) are compared for all images to show the relative impact of gating and synchronization. The line profile from the dead animal (Fig. 6e), presumably with no motion, is compared with the four gating schemes used for in vivo imaging, and demonstrates the relative importance of cardiac gating and ventilation synchronization. At the diaphragm/liver edge, the lack of ventilation synchronization clearly shows a

Table 3
Global Results of Cardiac Motion Study*

Gating scheme	Bead position (SD, microns)	
	Ventrodorsal projection	Lateral projection
Late expiration, acquisition in pre-systole ($N = 3$, 8 experiments)	38.5	26.8
Late expiration, acquisition in diastole ($N = 3$, 7 experiments)	29.8	45.3

*For each gating scheme, the SD is presented in microns averaged across all animals.

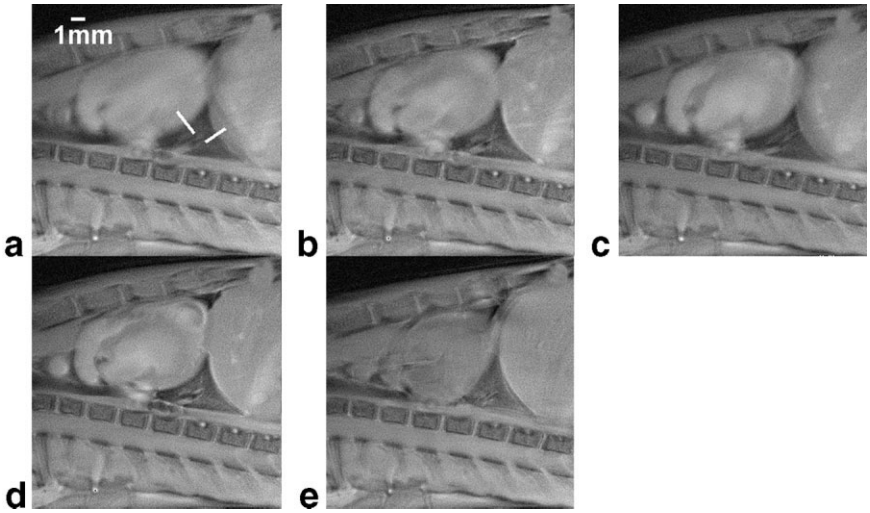

FIG. 6. Mid-sagittal MR images of a rat show the impact of the several gating methods: (**a**) no gating, (**b**) scan synchronous ventilation only, (**c**) cardiac gating only, (**d**) scan synchronous ventilation and cardiac gating, and (**e**) dead animal. The bars in **a** define the positions across the heart and diaphragm used to extract the line plots shown in Fig. 7.

flatter slope of the line profile than ventilation synchronized images or the dead animal images, emphasizing the importance of ventilation synchrony in edge sharpness. The cardiac boundary is clearly improved by cardiac gating, as evidenced by the steeper slope in both cardiac-gated images. The lower slope from the ventricle to the lung in the dead-animal image appears to be related to the postmortem reduction in overall contrast difference between these two regions.

DISCUSSION

To our knowledge, this is the first study to explore the reproducibility of the position of the diaphragm and heart in cardiac-gated, ventilation-synchronized studies in the rodent. We believe this reproducibility will define the ultimate barrier to increased spatial resolution for thoracic structures and the upper abdomen in MR microscopy. Several studies have been reported in rats and mice with Nyquist-limited spatial resolution under 100 μm (10,11,13). Since the penalty for higher spatial resolution is reduced SNR, it makes little sense to image at this resolution (100 μm) if in fact the motion blur is greater. The noise in MRI is not Poisson, so one cannot simply filter a motion-blurred image to recover lost signal. It is critical that we understand the magnitude of the motion-induced resolution loss so that we do not try to image beyond the spatial resolution that the biology will support.

The diaphragm moves more through the course of an extended MR study than any other part of the body. Thus the rationale for looking at the reproducibility of its position should be clear. Cardiac motion represents the next major barrier to improved resolution in the thorax. While other motion (peristalsis or blood pulsation) exists, we chose to limit these studies to areas in which we can have confidence in the measurement methods used.

In the diaphragm motion study, ventilation synchronous images demonstrated that the dome bead had a greater variability in returning to the same position compared to the beads on the lateral portions of the diaphragm. The greater variability is no doubt related to the proximity of this position of the diaphragm to the cardiac apex, which induces motion independently of the breathing cycle. We hypothesized that variability would be reduced by acquiring images that were synchronous with both the breathing cycle and the cardiac cycle. For this sequence, we had to define an "acquisition window." An X-ray image could actually be obtained any time during this 110-ms window, depending on the ECG trigger. During breath-hold, gas exchange continues to occur. The rates of alveolar diffusion between oxygen and carbon dioxide differ (alveolar oxygen diffuses 1.2 times more rapidly than alveolar carbon dioxide), and this is associated with a difference in the volumes of carbon dioxide and oxygen exchanged during breath-hold, and hence a change in alveolar and pulmonary volume (19). Consequently, we believe that over the 110-ms window, the lung volume does not remain constant, and therefore the position of the diaphragm is not the same at the beginning and end of the window. The effect of this change in lung volume during a brief breath-hold could be reduced by decreasing the acquisition window duration. However, this would significantly increase the acquisition time by decreasing the likelihood of a QRS occurring within the window. The amplitude of diaphragm motion is significantly reduced with the use of ventilation-synchronous acquisition strategies. As shown in Table 2, a displacement of up to 2 mm of the diaphragm can be expected without any synchronization to the breathing cycle. This highlights the importance of developing motion-control strategies for imaging moving organs, such as the lungs. Some authors have concluded that these strategies are time-consuming, and that acceptable results can be obtained without their use (8). This is true for studies in which general characteristics of the lung parenchyma, such as the mean T_2^* values, are evaluated. For studies that require an appreciation of the thoracic anatomy, gating and ventilatory sychronization are clearly beneficial.

The amplitude of the cardiac motion was less than the diaphragm motion. This supports our statement that the SDs observed in the diaphragm motion study were largely due to changes in lung volume during the acquisition window resulting in a larger variability in the diaphragm returning to the same position from image to image. Al-

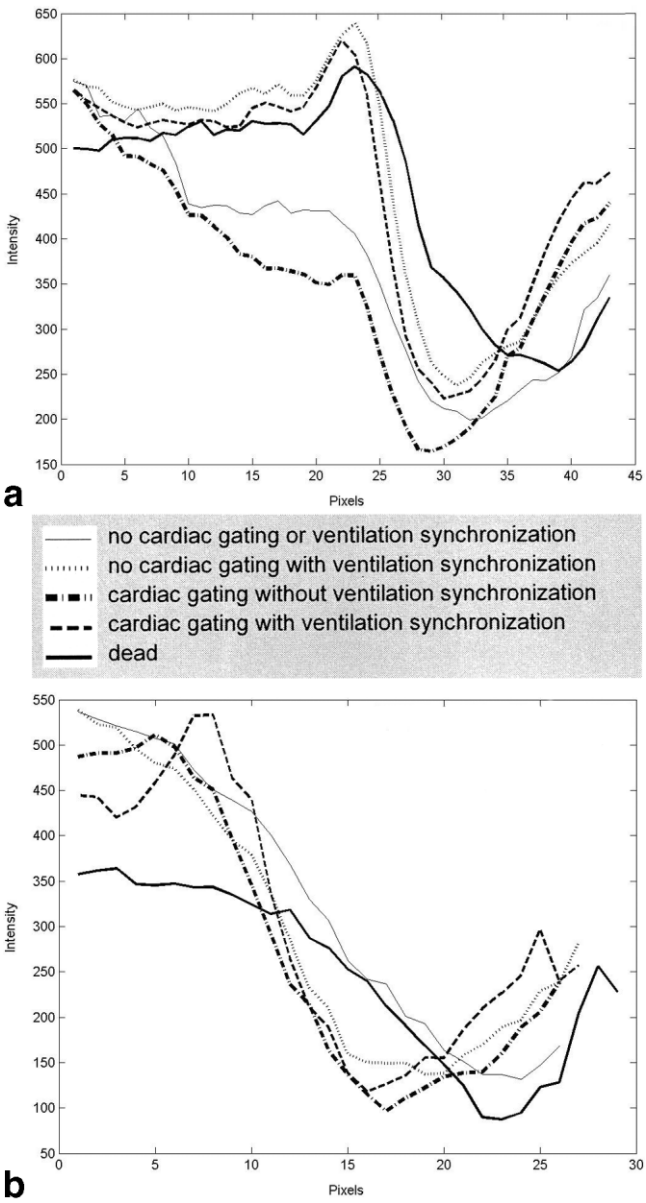

FIG. 7. Line profiles crossing the edges of the (**a**) diaphragm and (**b**) heart in all MR images with different gating schemes. **a:** Data are plotted from left to right from the liver into the lung parenchyma. **b:** Data are plotted from left to right from the ventricle into the lung parenchyma.

though breathing motion is known to induce a certain degree of motion of the heart and great vessels, the influence of a change in lung volume on the position of the heart is less than that on the position of the diaphragm. Reports from cineangiographic studies in humans show that during spontaneous breathing, the heart moves approximately half as much as the diaphragm (20). The heart is enclosed in the mediastinal space in the sagittal plane, and is less sensitive to lung motion than the diaphragm. This might account for the lower SDs we found in the cardiac motion study.

Our study shows that the techniques developed to control breathing motion and acquire ventilation-synchronous, cardiac-gated images allow the pulmonary and cardiac structures to return consistently to the same position each time data are acquired. The reproducibility of the position of the diaphragm is on the order of 50–100 μm, which is comparable to the spatial resolution limit imposed by the limited signal in the lung in MRI (11). For anatomic locations outside the thorax, there is a potential to achieve spatial resolution beyond 100 μm, if it is supported by the sensitivity of the method (21). As methods to improve sensitivity are developed, methods to limit the impact of motion must follow. This work defines the magnitude of the problem and provides some insight into how future improvements might be measured.

ACKNOWLEDGMENTS

The current work was performed at the Duke Center for In Vivo Microscopy, an NCRR National Resource (P41 RR05959). W.M. was supported in part by the French Ministry of Foreign Affairs (Lavoisier grant). We are grateful to Dr. Deborah Burstein at Beth Israel Deaconess Medical Center for very helpful discussions that led to this work.

REFERENCES

1. Callaghan PT, Eccles CD. Diffusion-limited resolution in nuclear magnetic resonance microscopy. J Magn Reson 1988;78:1–8.
2. Callaghan PT. Susceptibility-limited resolution in nuclear magnetic resonance microscopy. J Magn Reson 1990;87:304–318.
3. Callaghan PT, Eccles CD. Sensitivity and resolution in NMR imaging. J Magn Reson 1987;71:426–445.
4. Hedlund LW, Deitz J, Nassar R, Herfkens R, Vock P, Dahlke J, Kubek R, Effmann E, Putman C. A ventilator for magnetic resonance imaging. Invest Radiol 1986;21:18–23.
5. Hedlund LW, Cofer GP, Owen SJ, Allan Johnson G. MR-compatible ventilator for small animals: computer-controlled ventilation for proton and noble gas imaging. Magn Reson Imaging 2000;18:753–759.
6. Cassidy PJ, Schneider JE, Grieve SM, Lygate C, Neubauer S, Clarke K. Assessment of motion gating strategies for mouse magnetic resonance at high magnetic fields. J Magn Reson Imaging 2004;19:229–237.
7. Gewalt SL, Glover GH, Hedlund LW, Cofer GP, MacFall JR, Johnson GA. MR microscopy of the rat lung using projection reconstruction. Magn Reson Med 1993;29:99–106.
8. Beckmann N, Tigani B, Mazzoni L, Fozard JR. MRI of lung parenchyma in rats and mice using a gradient-echo sequence. NMR Biomed 2001; 14:297–306.
9. Hedlund LW, Johnson GA, Mills GI. Magnetic resonance microscopy of the rat thorax and abdomen. Invest Radiol 1986;21:843–846.
10. Fayad ZA, Fallon JT, Shinnar M, Wehrli S, Dansky HM, Poon M, Badimon JJ, Charlton SA, Fisher EA, Breslow JL, Fuster V. Noninvasive in vivo high-resolution magnetic resonance imaging of atherosclerotic lesions in genetically engineered mice. Circulation 1998;98:1541–1547.
11. Johnson GA, Cofer GP, Hedlund LW, Maronpot RR, Suddarth SA. Registered ^{1}H and ^{3}He magnetic resonance microscopy images of the lung. Magn Reson Med 2001;45:365–370.
12. Wiesmann F, Ruff J, Hiller KH, Rommel E, Haase A, Neubauer S. Developmental changes of cardiac function and mass assessed with MRI in neonatal, juvenile, and adult mice. Am J Physiol Heart Circ Physiol 2000;278:H652–H657.
13. Wiesmann F, Szimtenings M, Frydrychowicz A, Illinger R, Hunecke A, Rommel E, Neubauer S, Haase A. High-resolution MRI with cardiac and respiratory gating allows for accurate in vivo atherosclerotic plaque visualization in the murine aortic arch. Magn Reson Med 2003;50:69–74.
14. Nahrendorf M, Hiller KH, Hu K, Ertl G, Haase A, Bauer WR. Cardiac magnetic resonance imaging in small animal models of human heart failure. Med Image Anal 2003;7:369–375.

15. Brau ACS, Wheeler CT, Hedlund LW, Johnson GA. The fiber optic stethoscope: a cardiac monitoring and gating system for magnetic resonance microscopy. Magn Reson Med 2002;47:314–321.
16. Hedlund LW, Johnson GA. Mechanical ventilation for imaging the small animal lung. ILAR J 2002;43:159–174.
17. Qiu H, Cofer GP, Hedlund LW, Johnson GA. Automated feedback control of body temperature for small animal studies with MR microscopy. IEEE Trans Biomed 1997;44:1107–1113.
18. Brau ACS, Hedlund LW, Johnson GA. Cine magnetic resonance microscopy of the rat heart using cardiorespiratory-synchronous projection reconstruction imaging. J Magn Reson Imaging 2004;20:31–38.
19. Des Jardins TR. Cardiopulmonary anatomy and physiology: essentials for respiratory care. Albany, NY: Delmar Thomson Learning; 2002. 550 p.
20. Bogren HG, Lantz BM, Miller RR, Mason DT. Effect of respiration on cardiac motion determined by cineangiography. Implications concerning three-dimensional heart reconstruction using computer tomography. Acta Radiol Diagn (Stockh) 1977;18:609–620.
21. Miller JR, Hurlston SE, Face DW, Kountz DJ, MacFall JR, Hedlund LW, Ma QY, Johnson GA. Performance of a high-temperature superconducting probe for in vivo microscopy at 2.0 T. Magn Reson Med 1999;41:72–79.